

SCIENTIFIC REPORTS

OPEN

2 μm emission properties and nonresonant energy transfer of Er^{3+} and Ho^{3+} codoped silicate glasses

Ruijie Cao¹, Yu Lu¹, Ying Tian¹, Feifei Huang¹, Yanyan Guo², Shiqing Xu¹ & Junjie Zhang¹

Received: 13 June 2016
 Accepted: 01 November 2016
 Published: 30 November 2016

2.0 μm emission properties of $\text{Er}^{3+}/\text{Ho}^{3+}$ codoped silicate glasses were investigated pumped by 980 nm LD. Absorption spectra were determined. Intense mid-infrared emissions near 2 μm are observed. The spectral components of the 2 μm fluorescence band were analyzed and an equivalent model of four-level system was proposed to describe broadband 2 μm emission. Low OH^- absorption coefficient (0.23 cm^{-1}), high fluorescence lifetime (2.95 ms) and large emission cross section ($5.61 \times 10^{-21} \text{ cm}^2$) corresponding to Ho^{3+} : $^5\text{I}_7 \rightarrow ^5\text{I}_8$ transition were obtained from the prepared glass. Additionally, energy transfer efficiency from the Er^{3+} : $^4\text{I}_{13/2}$ to the Ho^{3+} : $^5\text{I}_7$ level can reach as high as 85.9% at 0.75 mol% Ho_2O_3 doping concentration. Energy transfer microscopic parameters (C_{DA}) via the host-assisted spectral overlap function were also calculated to elucidate the observed 2 μm emissions in detail. Moreover, the rate equation model between Er^{3+} and Ho^{3+} ions was developed to elucidate 2 μm fluorescence behaviors with the change of Ho^{3+} concentration. All results reveal that $\text{Er}^{3+}/\text{Ho}^{3+}$ codoped silicate glass is a promising material for improving the Ho^{3+} 2.0 μm fiber laser performance.

Over the past several years, numerous efforts have been devoted to obtain efficient and powerful mid-infrared lasers operating in the eye-safe 2 μm wavelength region. This is due to their wide applications such as coherent laser radar systems, medical surgery, laser imaging, remote chemical sensing and pump sources for mid-infrared lasers as well as optical communication systems^{1–3}.

Usually, Tm^{3+} -doped, Ho^{3+} -doped, and Raman fiber lasers are the most widespread way of getting 2-micron laser output. In 2010, three all-fiber Ho^{3+} -doped lasers emitting in the range of 2050–2100 nm were fabricated. The lasers were pumped by an Yb^{3+} doped fiber laser at 1147 nm with a power up to 35 W⁴. For all the lasers tested, the output power was found to be as high as 10 W, the slope efficiency being 30%. In 2015, lasing at 2.077 μm is also obtained from a 27 cm long Ho^{3+} doped fluorotellurite microstructured fiber. The maximum unsaturated power is about 161 mW and the corresponding slope efficiency is up to 67.4%⁵. Using ultra short (1.6 cm) as-drawn highly Tm^{3+} doped barium gallo-germanate (BGG) single mode (SM) fiber, a single-frequency fiber laser at 1.95 μm has been demonstrated with a maximum output power of 35 mW when in-band pumped by a home-made 1568 nm fiber laser in 2015⁶. In addition, in 2010, a multiple-watt $\text{Tm}^{3+}/\text{Ho}^{3+}$ codoped aluminosilicate glass fiber laser operating in narrowband (<0.5 nm) and tuned across a range exceeding 280 nm was also presented⁷. However, Raman fiber laser requires high power pump sources in the spectral range, which is a shortcoming in the view of practical applications⁴. The Tm^{3+} doped sources are typically limited to efficient operation at <2.05 μm ⁸, although Tm^{3+} doped fiber lasers with high output power and slope efficiency have been demonstrated in silica⁹, silicate¹⁰ and germanate fibers¹¹. In such case, the transition ($^5\text{I}_7 \rightarrow ^5\text{I}_8$) of Ho^{3+} ions produces radiation in the range of 2.05 μm to 2.2 μm ¹², which could totally match the applications which require good atmospheric propagation. Moreover, atmospheric transmission spectra provided by ModTran⁸ show the advantage of operating at wavelength beyond 2.1 μm in comparison to the windows accessible thulium sources. Therefore, it is expected that Ho^{3+} activated glasses are promising candidates for 2 μm fiber laser. But the lack of efficient absorption band at the 980 nm wavelength suggests that Ho^{3+} ions cannot be pumped by high-power and commercial 980 nm laser diodes (LDs). Fortunately, Yb^{3+} or Er^{3+} ions can be codoped to improve the absorption band of Ho^{3+} ions at 980 nm. In particular, Ho^{3+} doped glasses sensitized by Yb^{3+} are recognized as efficient systems for obtaining strong luminescence in both the infrared and visible range of the spectrum^{13,14}. This is due to

¹College of Materials Science and Engineering, China Jiliang University, Hangzhou 310018, P.R. China. ²Collage of Materials Science and Engineering, Changchun University of Science and Technology, Changchun, 130022, P.R. China. Correspondence and requests for materials should be addressed to S.X. (email: shiqingxu@cjl.u.edu.cn) or J.Z. (email: jjzhang@cjl.u.edu.cn)

the large absorption and emission cross-section, relatively long lifetime, and simply energy level scheme of Yb^{3+} . Moreover, Yb^{3+} can be efficiently pumped by a laser diode (LD) near 980 nm which is one of the most popular and convenient commercial pump sources. So far, $\text{Ho}^{3+}/\text{Yb}^{3+}$ codoped glasses^{13–15} have been investigated by researchers. But, compared with Yb^{3+} ions, Er^{3+} : $^4\text{I}_{13/2}$ level can match better with Ho^{3+} : $^5\text{I}_7$ level, which is more beneficial for 2 μm emissions¹⁶. Hence, it can be expected that 2 μm fluorescence can be obtained from the $\text{Er}^{3+}/\text{Ho}^{3+}$ codoped sample pumped by 980 nm excitation and there is a rare investigation focused on the 2.0 μm emission obtained from the $\text{Er}^{3+}/\text{Ho}^{3+}$ codoped pumped by 980 nm excitation.

In order to get powerful mid-infrared emissions from Ho^{3+} , the host glass is another factor to be considered as important as the sensitizer. Multi-component silicate glass is a promising material in realizing 2 μm lasers. Compared to silica glass, it has a less-defined glass network, which can provide a higher solubility of rare earth ions¹⁷. In some cases, single-frequency laser operation for example, a much shorter fiber is required to achieve high gain ability¹⁸. Here silicate glass is a more appropriate material than silica glass. Though the larger multiphonon relaxation rate induced by higher phonon energy in silicate glass ($\sim 1050 \text{ cm}^{-1}$) compared with other multi-component glasses such as fluoride and heavy metal glasses (e.g., germanate, telluride, bismuth glasses), lower quantum efficiency of $\sim 2 \mu\text{m}$ luminescence, it turns out that slope efficiency in the silicate fiber lasers can be much higher than that in other glass fibers lasers^{10,19,20}. In addition, it should be noted that in comparison with fluoride and heavy metal glasses, the main glass network of the silicate fiber is SiO_2 , which has strong mechanical strength, high damage threshold and better compatibility with conventional passive silica fibers.

To the best of our knowledge, few reports on 2 μm fluorescence properties in $\text{Er}^{3+}/\text{Ho}^{3+}$ codoped silicate glass have been carried out, and it is focused mainly on the spectroscopic properties of lead silicate excited by 800 and 1550 nm LD¹⁶. But in this work, not only 2 μm spectroscopic properties of Ho^{3+} are investigated in $\text{Er}^{3+}/\text{Ho}^{3+}$ codoped silicate glasses pumped by 980 LD. But also the energy transfer mechanism between Ho^{3+} and Er^{3+} was analyzed based on the built phonon-assisted energy transfer analysis, which is helpful to optimize and ensure the technological applications of the codoped materials. Moreover, the rate equation model between Er^{3+} and Ho^{3+} ions was also developed to quantitatively elucidate 2 μm fluorescence behaviors. This work reveals that $\text{Er}^{3+}/\text{Ho}^{3+}$ codoped silicate glass is a promising material for improving the Ho^{3+} 2.0 μm fiber laser performance and may provide useful guidance for the design of other mid-infrared laser materials.

Experimental

$\text{Er}^{3+}/\text{Ho}^{3+}$ codoped silicate glasses were synthesized by conventional melting method, which has the following molar compositions: $(55-x)\text{SiO}_2-5\text{Al}_2\text{O}_3-7\text{CaO}-3\text{CaF}_2-13\text{BaCO}_3-15\text{BaF}_2-1\text{La}_2\text{O}_3-1\text{Er}_2\text{O}_3-x\text{Ho}_2\text{O}_3$, ($x = 0.25, 0.5, 0.75, 1.0$) denoted as SEH0.25, SEH0.5, SEH0.75 and SEH1.0, respectively. At the same time, Ho^{3+} , Er^{3+} singly doped and non doped sample were also prepared to make a comparison and denoted as SH, SEH0 and S. Samples were synthesized by using high-purity SiO_2 , Al_2O_3 , CaO , CaF_2 , BaCO_3 , BaF_2 , La_2O_3 , Er_2O_3 (99.99%) and Ho_2O_3 (99.99%) powders. Raw materials (20 g) were mixed homogeneously and melted in a platinum crucible with a SiC-resistance electric furnace at the temperature of 1400 °C for 60 min. Then the melts were quenched on preheated stainless steel plate and annealed at 10 °C below the glass transition temperature for 2 h, then cooled to room temperature. Finally, the annealed samples were fabricated and optically polished to the size of $10 \times 10 \times 1.5 \text{ mm}^3$ for the optical property measurement.

The densities (3.76 g/cm^3) were tested by Archimedes principle using distilled water as an immersion liquid with error limit of $\pm 0.05\%$. The refractive index of the host glass was measured by the prism minimum deviation method at three wavelengths, 633, 1311 and 1539 nm, and they are 1.6111, 1.6051, and 1.5995, respectively. The resolution of the instrument is $\pm 0.5 \times 10^{-4}$. The standard deviation in refractive index at different points of the same glass is around $\pm 1 \times 10^{-4}$. The refractive index dispersion curve was calculated by Cauchy's formula $n(\lambda) = a + b/\lambda^2 + c/\lambda^4$, where a , b and c are found to be 1.5806, 5.0124×10^4 and -1.5269×10^{10} respectively. Absorption spectra were determined by means of a Perkin Elmer Lambda 900UV-VIS-NIR spectrophotometer in the range of 300–2200 nm with the resolution of 1 nm. Photoluminescence spectra in the ranges of 1750–2300 nm were measured with steady state spectrometer (FLSP 980) (Edingburg Co., England) and detected with a liquid-nitrogen-cooled PbS detector using an 980 nm laser diode (LD) as an excitation source. The fluorescence lifetimes of the 2 μm (Ho^{3+} : $^5\text{I}_7$ state), and 1.53 μm (Er^{3+} : $^4\text{I}_{13/2}$ state) were measured with light pulse of the 980 nm LD and an HP546800B 100-MHz oscilloscope. In addition, the mid-infrared transmission spectra was obtained by using a Thermo Nicolet (Nexus FT-IR Spectrometer) spectrophotometer in the range of 2.6–3.6 μm with resolution of 4 cm^{-1} . The same experimental conditions for different samples were maintained so as to get comparable results. All the measurements were performed at ambient temperature.

Results

Absorption spectra and infrared transmittance spectrum. The room temperature absorption spectra of Er^{3+} , Ho^{3+} singly doped and $\text{Er}^{3+}/\text{Ho}^{3+}$ codoped silicate glasses were obtained within the wavelength region of 300–2200 nm as presented in Fig. 1. The absorption bands at wavelength shorter than 300 nm are not observed due to the intrinsic band-gap absorption of host glass. The absorption spectra are characterized by Er^{3+} absorption bands from the $^4\text{I}_{15/2}$ level to different excited levels of $^4\text{I}_{13/2}$, $^4\text{I}_{11/2}$, $^4\text{I}_{9/2}$, $^4\text{F}_{9/2}$, $^4\text{S}_{3/2}$, and $^4\text{F}_{7/2}$, along with absorption transitions of Ho^{3+} from the ground state ($^5\text{I}_8$) to higher levels of $^5\text{I}_7$, $^5\text{I}_6$, $^5\text{F}_5$ and $^5\text{F}_4+^5\text{S}_2$, respectively. No obvious divergences can be found in the shape and peak positions of the absorption bands between singly doped and codoped samples, which revealed that both Ho^{3+} and Er^{3+} ions are homogeneously imbedded into the glassy network without apparent clusters in the prepared silicate glasses. Besides, for the absorption spectrum of Ho^{3+} singly doped sample, it is noted that few absorption bands can match well with readily available laser diodes, such as 808 and 980 nm. Fortunately, $\text{Er}^{3+}/\text{Ho}^{3+}$ codoped sample displays an obvious absorption band around 980 nm owing to the absorption transition of Er^{3+} : $^4\text{I}_{15/2} \rightarrow ^4\text{I}_{11/2}$. Therefore, the prepared $\text{Er}^{3+}/\text{Ho}^{3+}$ codoped silicate glass can be excited by commercially 980 nm LD.

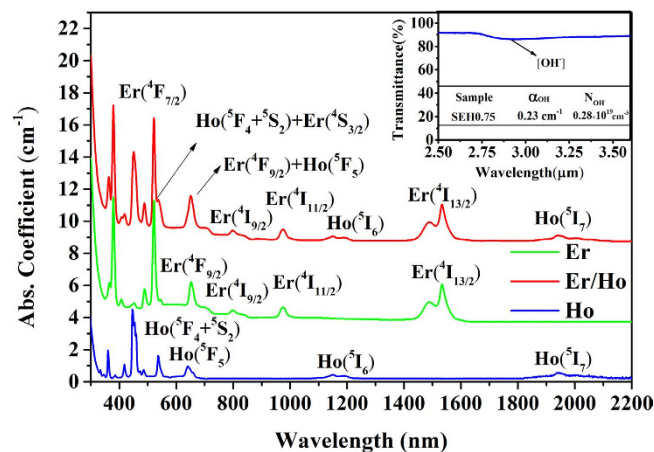


Figure 1. Absorption spectra of Er^{3+} , Ho^{3+} singly doped and $\text{Er}^{3+}/\text{Ho}^{3+}$ codoped silicate glasses. The inset is infrared transmittance spectrum of prepared sample.

The inset in Fig. 1 shows the infrared transmittance spectrum of SEH0.75 sample at 1.5 mm thick. The transmittance reaches as high as 91% (the 9% loss may be attributed to the Fresnel reflection dispersion and absorption of the glass). It is noted that the absorption band at 3 μm is apparent, which can be ascribed to the vibration of hydroxyl groups. Here, the free OH^- group, whose fundamental vibration ranges between 2500 and 3600 cm^{-1} (2.7~4 μm), is one of the dominant quenching centers in Ho^{3+} doped glass. It is because the energy gap of the $^5\text{I}_7 \rightarrow ^5\text{I}_8$ (~5100 cm^{-1}) transition is corresponding to the energy of the first overtone (5000~7200 cm^{-1} , 1.35~2 μm) of the fundamental stretching vibration of the OH^- groups. So a Ho^{3+} ion is coupled to free OH^- groups, non-radiative relaxation of one OH^- vibration quanta. Therefore, the contents of OH^- groups have an influence on mid-infrared fluorescence since residual hydroxyl groups in glasses can act as the fluorescence-quenching center. The absorption coefficient α_{OH^-} (cm^{-1}) in the glass network can be evaluated with the following equation²¹:

$$\alpha_{\text{OH}^-} = \frac{\ln(T/T_0)}{l} \quad (1)$$

where l is the thickness of the sample, T , T_0 are the maximum transmittance and the transmittance around 3 μm , respectively. In addition, the OH^- concentration (N_{OH^-}) in the glass network can also be evaluated with the following equation²²:

$$N_{\text{OH}^-} = \frac{N_A}{\epsilon} \alpha_{\text{OH}^-} \quad (2)$$

The value ϵ is the molar absorptivity corresponding to OH^- in silicate glasses ($49.1 \times 10^3 \text{ cm}^2/\text{mol}$)²² and N_A is the Avogadro constant ($6.02 \times 10^{23}/\text{mol}$). The absorption coefficient α_{OH^-} (cm^{-1}) and OH^- concentration (N_{OH^-}) of the SEH0.75 sample are 0.23 cm^{-1} and $0.28 \times 10^{19} \text{ cm}^{-3}$, respectively, which are significantly lower than the reported values of tellurite glass²³ and comparable to these of germanate-tellurite²¹ and germanate glass²⁴. Thus, it is expected that better spectroscopic properties will be obtained. In addition, a lower OH^- content could be obtained under a controlled atmosphere and a melting procedure in the future studied.

Analysis of fluorescence spectra at 2 μm . Figure 2 presents fluorescence spectra of Er^{3+} , Ho^{3+} singly doped and $\text{Er}^{3+}/\text{Ho}^{3+}$ codoped silicate glasses in the region of 1750~2300 nm pumped at 980 nm. All the samples were measured under the same conditions. No emission peaks can be observed for Er^{3+} singly doped sample. Due to Ho^{3+} ions do not absorb 980 nm photons, 2.0 μm emission peaks of Ho^{3+} single doped glass can't also be obtained although presence of $\text{Ho}^{3+} ^5\text{I}_7 \rightarrow ^5\text{I}_8$ transition. However, obvious 2 μm emission peaks can be found in the $\text{Er}^{3+}/\text{Ho}^{3+}$ codoped system, which is due to the presence of an energy transfer process from Er^{3+} to Ho^{3+} ions (this energy transfer phenomenon will be described in a later section). Moreover, with increasing Ho^{3+} concentration, the fluorescent intensity increases firstly and then decreases monotonically as presented in the inset of Fig. 2. The optimal Ho^{3+} concentration is located at 0.5 mol% ($0.93 \times 10^{20} \text{ ions}/\text{cm}^3$) and the decreased 2 μm emissions are owing to the concentration quenching.

From Fig. 3, it is worth mentioning that 2 μm fluorescence band shows broad non-Gaussian peak shape and wider emission band, which may have potential application in mid-infrared fiber amplifier and broad band tunable lasers. It is therefore noteworthy to understand the factors, which control the intensity and the width of the band at almost 2 μm . For this reason, it is important to know that this band results from the electronic transition between the 7 and 8 Stark sublevels the first excited state $^5\text{I}_7$, and the ground state $^5\text{I}_8$ respectively. To verify the spectral components of 2 μm emission peak, the Gaussian deconvolution procedure is carried out and the result is displayed in Fig. 3. Since the gap between two Stark sublevels is usually much lower than that existing between two neighboring J levels of a free rare earth ion, transitions between the different Stark levels are close in energy and it is not possible to clearly resolve them separately. Therefore, transition lines overlap and appear to form a single large band as observed in Fig. 3. In reality, the gap between two Stark sublevels depend on the electric

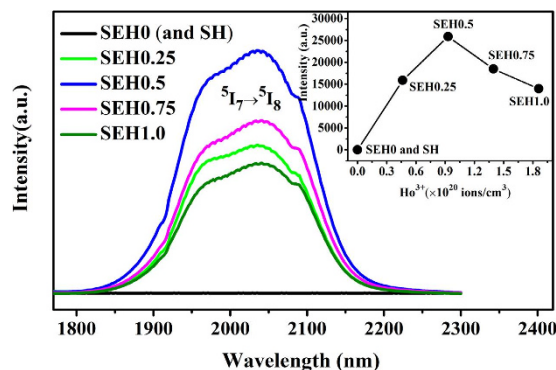


Figure 2. 2 μm fluorescence spectra of Er^{3+} , Ho^{3+} singly doped and $\text{Er}^{3+}/\text{Ho}^{3+}$ codoped silicate glasses in the region of 1750–2300 nm pumped at 980 nm. The inset is 2 μm emission intensity dependence of Ho^{3+} concentration.

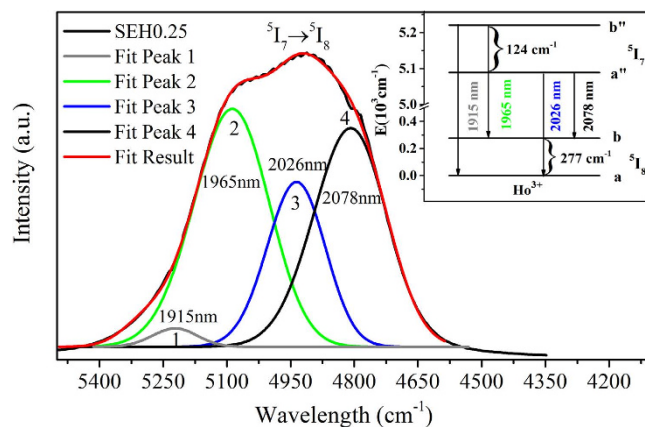


Figure 3. Deconvolution of 2 μm emission spectra of Ho^{3+} in silicate glass using Gaussian functions. The inset is an equivalent model of four-level system for describing the 2 μm fluorescence band.

crystal-field strength generated by the atoms of the surrounding medium and it is a sensitive indicator of the symmetry around Ho^{3+} ions in the host matrix. Indeed, the number of Stark levels increases when decreasing the site symmetry of Ho ions. In view of that, we found that a superposition of four bands with Gaussian profile is able to provide a good fit to the overall spectral line shape, as shown by the curves in Fig. 3. Here, it can be observed that the wavelengths of four Gaussian profiles are centered at 1915, 1965, 2026 and 2078 nm, respectively. To understand more comprehensively the four Stark emission bands, an equivalent model of four-level system (exclude the existence of non-equivalent optical centers) for describing the 2 μm fluorescence band is also revealed in the inset of Fig. 3. The ground state 5I_8 is composed of two Stark level of lower a and upper b. In the same way, the upper 5I_7 level contains two Stark level of lower a'' and upper b'' . Therefore, the four Stark emission bands centered at 1915, 1965, 2026 and 2078 nm are the peak 1, 2, 3 and 4 corresponding to the $b'' \rightarrow a$, $a'' \rightarrow a$, $b'' \rightarrow b$ and $a'' \rightarrow b$ transitions, respectively. From the observation of emission peak, it can be seen that the relative intensity of 2026 nm emission peak is the highest that the other peak in the glass indicating here is slight energy re-absorption at the considered dopant ions concentration. In addition, it can be calculated that the total Stark splitting energy of 5I_7 state is about 124 cm^{-1} , which is lower than that of 5I_8 level (277 cm^{-1}) in Ho^{3+} activated silicate glass. Moreover, the Gaussian peak positions have minor shifts in comparison to that of germanate glass²⁵, which indicate that the extent of the Stark splitting is closely dependent on the glass compositions.

Stimulated emission cross-section and 2 μm lifetime. Important parameters that used to estimate the emission ability of luminescent center for 2.0 μm emission transition ($^5I_7 \rightarrow ^5I_8$) include mainly emission cross section (σ_{em}). The maximum fluorescence peak intensity for the prepared silicate glass is observed around 0.5 mol% Ho^{3+} (SEH0.5 sample). Hence, the optimal 2.0 μm fluorescence spectra is selected to calculate emission cross sections. The emission cross section were subsequently calculated by the following Fuchtbauer-Ladenburg equation²⁶

$$\sigma_{em}(\lambda) = \frac{\lambda^4 A_{rad}}{8\pi c n^2} \times \frac{\lambda I(\lambda)}{\int \lambda I(\lambda) d\lambda} \quad (3)$$

where λ is the wavelength. A_{rad} is the spontaneous transition probability. $\lambda I(\lambda)$ is the emission spectrum, and n and c are the refractive index and light speed in value, respectively.

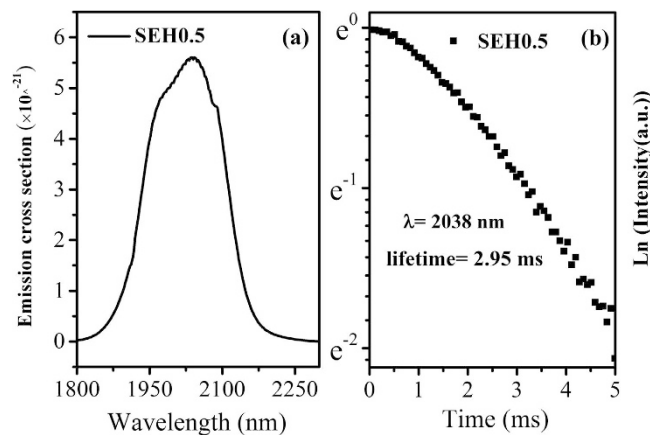


Figure 4. (a) $2\mu\text{m}$ emission cross section of $\text{Er}^{3+}/\text{Ho}^{3+}$ codoped silicate glass (SEH0.5 sample). (b) The $2\mu\text{m}$ lifetime of the SEH0.5 sample.

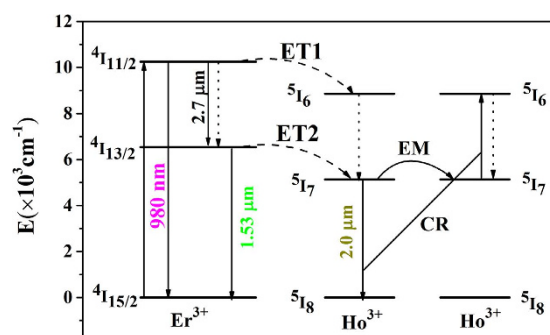


Figure 5. Energy level diagram and energy transfer mechanism between Er^{3+} and Ho^{3+} ions in silicate glass.

According to Eq. (3), the emission cross section is determined as depicted in Fig. 4(a). It can be seen that the peak of emission cross sections at $2.04\mu\text{m}$ is $5.61 \times 10^{-21} \text{ cm}^2$, which is higher than those of other silicate glass ($3.54 \times 10^{-21} \text{ cm}^2$)²⁷ and germanate-tellurite glass ($4.36 \times 10^{-21} \text{ cm}^2$)¹⁵ while slightly lower than that of germanate glass ($8.00 \times 10^{-21} \text{ cm}^2$)²⁸. Higher emission cross section is extremely useful for better laser actions²⁹. Moreover, it is interesting that the measured $2.04\mu\text{m}$ lifetime (2.95 ms) of the prepared glass was depicted in Fig. 4(b), which is more appropriate to evaluate the emission properties of laser glass, is larger than that of the germanosilicate glass (1.44 ms)³⁰ and tellurite glasses (1.6 ms)³¹. Therefore, the $\text{Er}^{3+}/\text{Ho}^{3+}$ codoped silicate glass, which possess large emission cross section and fluorescence lifetime, can be an excellent candidate in achieving intense $2.0\mu\text{m}$ emission.

Energy transfer mechanism and nonresonant energy transfer analysis. To elucidate the observed fluorescent phenomenon, energy level diagram and energy transfer mechanism are proposed based on previous investigation and depicted in Fig. 5.

The ions in the Er^{3+} : $4\text{I}_{15/2}$ level are pumped to a higher $4\text{I}_{11/2}$ level via ground state absorption (GSA: Er^{3+} : $4\text{I}_{15/2} + \text{a photon} \rightarrow 4\text{I}_{11/2}$) when excited by commercial 980 nm LD. On the one hand, the ions in the Er^{3+} : $4\text{I}_{11/2}$ level can relax to the lower $4\text{I}_{13/2}$ level by a nonradiative process and radiative relaxation ($2.7\mu\text{m}$ emissions). Then, the $4\text{I}_{13/2}$ level transfers a part of its energy to the adjacent Ho^{3+} : 5I_7 level (ET2: Er^{3+} : $4\text{I}_{13/2} + \text{Ho}^{3+}$: $5\text{I}_8 \rightarrow \text{Er}^{3+}$: $4\text{I}_{15/2} + \text{Ho}^{3+}$: 5I_7), making this energy level populated. In addition, some ions in the $4\text{I}_{13/2}$ level radiate to the ground state ($4\text{I}_{15/2}$), resulting in $1.53\mu\text{m}$ emissions (Er^{3+} : $4\text{I}_{13/2} \rightarrow 4\text{I}_{15/2} + 1.53\mu\text{m}$). On the other hand, the Er^{3+} : $4\text{I}_{11/2}$ level can also transfer its energy to the Ho^{3+} : 5I_6 level via an ET1 (Er^{3+} : $4\text{I}_{11/2} + \text{Ho}^{3+}$: $5\text{I}_8 \rightarrow \text{Er}^{3+}$: $4\text{I}_{15/2} + \text{Ho}^{3+}$: 5I_6) process. Subsequently, the populations in Ho^{3+} : 5I_6 level can relax radiatively or nonradiatively to the next 5I_7 level. Finally, $2\mu\text{m}$ emission takes place due to radiative transition to the ground state (5I_8 level) from Ho^{3+} : 5I_7 level (Ho^{3+} : $5\text{I}_7 \rightarrow 5\text{I}_8 + 2\mu\text{m}$). Furthermore, it is noted that $2\mu\text{m}$ emission can be quenched when Ho^{3+} concentration is more than optimal value (0.5 mol%) as revealed in Fig. 5, which may be attributed to the energy migration (EM: Ho^{3+} : $5\text{I}_7 \rightarrow 5\text{I}_7$) and cross relaxation (CR: Ho^{3+} : $5\text{I}_7 + 5\text{I}_7 \rightarrow 5\text{I}_6 + 5\text{I}_8$) processes.

Basing on discussions mentioned above, we can summarize that both ET1 and ET2 processes can generate $2\mu\text{m}$ fluorescence. However, from Fig. 6(a), it is found that the 980 nm emission intensity has no substantial change with increasing Ho^{3+} concentration while the $1.53\mu\text{m}$ emission intensity decreases quickly as displayed in Fig. 6(b). It is noted that the 980 nm emission of non doped sample (S) was synthesized and make comparison

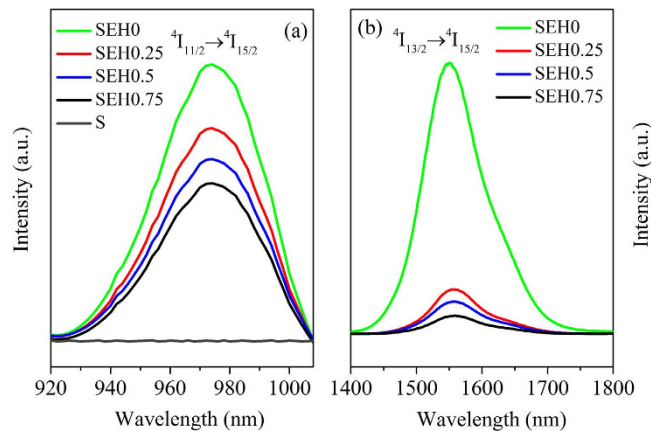


Figure 6. (a) 980 nm fluorescence spectra (b) 1.53 μm fluorescence spectra in non doped, Er^{3+} singly doped and $\text{Er}^{3+}/\text{Ho}^{3+}$ codoped silicate glasses pumped at 980 nm

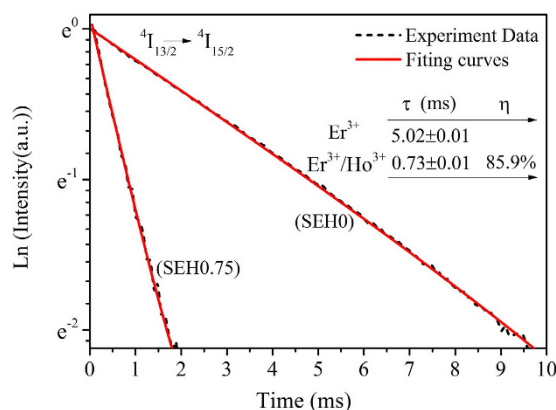


Figure 7. The decay curves at 1.53 μm in Er^{3+} singly and $\text{Er}^{3+}/\text{Ho}^{3+}$ codoped silicate glasses (the inset is lifetimes (τ) from single exponential fitting and energy transfer efficiency (η)).

with the samples (SEH0, SEH0.25, SEH0.5, and SEH0.75). It is found that the 980 nm emission intensity of sample S is much smaller than those of the samples (SEH0, SEH0.25, SEH0.5, and SEH0.75). Therefore, it can be confirmed that the excitation radiation almost have almost no effect on the resulting 980 nm spectra and can be ignored as presented in Fig. 6(a). Thus, it can be concluded that ET2 is much more efficient in comparison to ET1 process. Hence, enhanced 2 μm emission can be mainly ascribed to ET2 process.

In order to estimate the energy transfer (ET2) efficiency and rate from $\text{Er}^{3+}: 4\text{I}_{13/2}$ to $\text{Ho}^{3+}: 5\text{I}_7$ level, the ion lifetimes in $\text{Er}^{3+}: 4\text{I}_{13/2}$ level with and without Ho^{3+} ions have been determined from Fig. 7. The lifetimes were determined by single exponential fitting procedure, as listed in the inset of Fig. 7 as well as the energy transfer efficiency (η). The energy transfer rate (W_{ET}) and energy transfer efficiency (η) were evaluated by using the following equation^{32–34}

$$W_{\text{ET}} = \frac{1}{\tau} - \frac{1}{\tau_0} \quad (4)$$

$$\eta = 1 - \frac{\tau}{\tau_0} \quad (5)$$

where τ , τ_0 are lifetimes of $\text{Er}^{3+}: 4\text{I}_{13/2}$ with codoping 0.75 mol% Ho^{3+} and without Ho^{3+} ions, respectively. The derived maximum energy transfer rate is found to be 1170.6 s^{-1} as well as the energy transfer efficiency (η) of 85.9%. The higher η , compared with fluorotellurite glasses (67.33%)³⁵ and fluoride glass (45%)³⁶, is beneficial for the design of 2 μm laser under readily available high power, compact diode laser pumping (980 nm LD). Besides, the fluorescence quantum efficiency has been estimated from the lifetime values by the following equation

$$\eta = \frac{\tau_{\text{exp}}}{\tau_R} \times 100\% \quad (6)$$

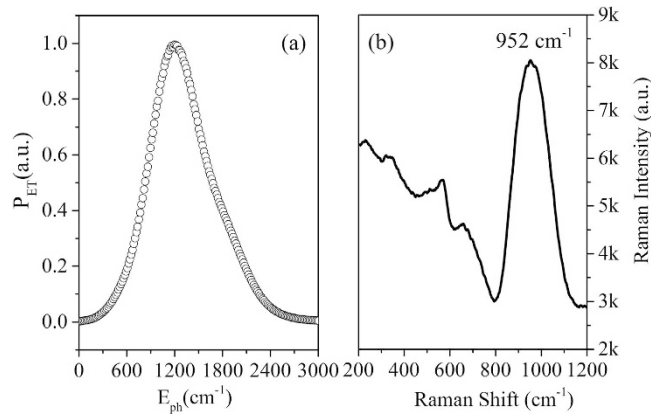


Figure 8. (a) Energy transfer probability (P_{ET}) vs Phonon energy in the codoped glass. (b) Raman spectra of SEH0.75glass sample.

where τ_{exp} is the measured fluorescence lifetime of the sample (SEH0.5), and τ_R is the theoretical lifetime the sample (SEH0.5), which were estimated from the absorption spectrum and J-O intensity parameters and can be calculated by the formula provided in ref. 14. The measured 5I_7 lifetime (2.95 s) for Ho^{3+} is shorter than the calculated lifetime (3.74 s), which is due to non-radiative quenching. It can be found that the fluorescence quantum efficiency is high as 78.88%, which is comparable to that of fluoride glass (80.35%)³⁷. Therefore, Er^{3+}/Ho^{3+} codoped silicate glass is a more promising material for improving the Ho^{3+} 2.0 μm fiber laser performance.

The extent of energy transfer (ET2) from the Er^{3+} : $^4I_{13/2}$ to the Ho^{3+} : 5I_7 level is dependent on the spectral overlap of the donor's emission (Er^{3+}) with the acceptor's absorption (Ho^{3+}). Although, the higher energy transfer (ET2) efficiency ($\eta = 85.9\%$) has been confirmed, the spectral overlap between the 1.53 μm emissions of Er^{3+} and 2 μm absorptions of Ho^{3+} is very poor, with an energy gap of $\sim 1400\text{ cm}^{-1}$, which suggests that the energy transfer process in the Er^{3+}/Ho^{3+} codoped silicate glass system may be assisted by host phonons. For such a nonresonant energy transfer, the Dexter model can be generalized to the nonresonant phonon assisted energy transfer case taking account of phonon energy involved (E_{ET}) as well as the phonon density. The energy transfer probability (P_{ET}) can be estimated by the phonon-modified spectral overlap integral, $I(E_{ph})$ as follows³⁸:

$$P_{ET} \propto I(E_{PH}) = \frac{e^{E_{PH}/k_B T}}{e^{E_{PH}/k_B T} - 1} \int \frac{f_D(E - E_{ph})f_A(E)}{E^2} dE \quad (7)$$

where E_{ph} is the phonon energy of host, k_B is Boltzmann constant, and T is absolute temperature. According to the 1.53 μm emission cross section spectra of Er^{3+} and 2 μm absorption of Ho^{3+} absorption cross section spectra, the normalized energy transfer probability has been calculated as a function of phonon energy in the range of 0 \sim 3000 cm^{-1} as presented in Fig. 8(a). It can be observed that the normalized energy transfer probability (P_{ET}) increases with an increase in phonon energy and it reaches a maximum for the phonons energy around 1200 cm^{-1} . Then, the energy transfer probability (P_{ET}) decreases and diminishes with further increase in the phonon energy. Thus, the energy difference between the energy levels of $^4I_{13/2}$ (Er^{3+}) and 5I_7 (Ho^{3+}) can be bridged by the host phonons for an efficient energy transfer. As maximum phonon energy of present silicate glass (SEH0.75glass) is $\sim 952\text{ cm}^{-1}$, as presented in Fig. 8(b), so about one or two phonon is required to bridge the energy gap between Er^{3+} : $^4I_{13/2}$ and Ho^{3+} : 5I_7 state. Assisted with the host phonon, the energy level mismatch ($\sim 1400\text{ cm}^{-1}$) can be covered. It can be expected that the high phonon energy hosts like silicate glasses, can promote the energy transfer from energy levels of $^4I_{13/2}$ (Er^{3+}) to 5I_7 (Ho^{3+}) with less number of phonons. But considering that higher phonon energy also lead to higher non-radiative relaxation of 5I_7 level of Ho^{3+} and less probability of 2 μm emission. Hence, the silicate material with moderate phonon energy is important for highly efficient 2 μm emissions in Er^{3+}/Ho^{3+} codoped samples.

To understand more intuitively and clearly the phonon assisted energy transfer mechanism from Er^{3+} to Ho^{3+} , emission cross sections of Er^{3+} : $^4I_{11/2} \rightarrow ^4I_{15/2}$ transition with the participation of m phonons ($m = 0, 1$ and 2) and absorption cross sections of Ho^{3+} : $^5I_8 \rightarrow ^5I_6$ transition in prepared sample are depicted in Fig. 9(a), meanwhile, emission cross sections of Er^{3+} : $^4I_{13/2} \rightarrow ^4I_{15/2}$ transition with the participation of m phonons ($m = 0, 1$ and 2) and absorption cross sections of Ho^{3+} : $^5I_8 \rightarrow ^5I_7$ transition in prepared samples are depicted in Fig. 9(b). The emission cross section with the participation of m phonons can be determined by following equation³⁹:

$$\delta_{em}^{stokes} = \delta_{em} \frac{S_0 e^{-s_0}}{m!} \left[\frac{1}{e^{h\nu/k_B T} - 1} + 1 \right] \quad (8)$$

where σ_{em} is the emission cross section of Er^{3+} : $^4I_{11/2} \rightarrow ^4I_{15/2}$, $^4I_{13/2} \rightarrow ^4I_{15/2}$ transitions, which is equal to the one with zero-phonon calculated by the Mc-Cumber equation³⁹ and S_0 is the Huang-Rhys factor, which is 0.31 for rare earth ions³⁸. Such as the above, $h\nu_{max}$ is the maximum phonon energy of host and k is Boltzmann constant. Although, there is almost no spectral overlapping between Er^{3+} : $^4I_{11/2} \rightarrow ^4I_{15/2}$ and Ho^{3+} : $^5I_8 \rightarrow ^5I_6$ transitions as well as that between Er^{3+} : $^4I_{13/2} \rightarrow ^4I_{15/2}$ and Ho^{3+} : $^5I_8 \rightarrow ^5I_7$ transitions without the participation of phonons, a

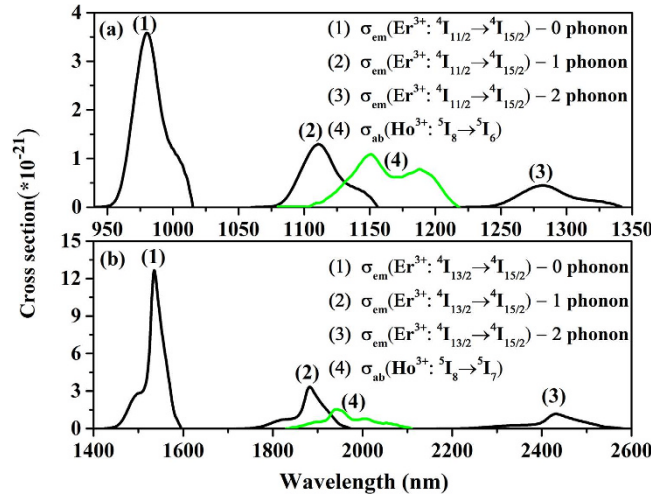


Figure 9. (a) Emission cross sections assisted by m ($m = 0, 1$ and 2) phonons for the $\text{Er}^{3+}: 4I_{11/2} \rightarrow 4I_{15/2}$ transition and absorption cross sections for the $\text{Ho}^{3+}: 5I_8 \rightarrow 5I_6$ transition; (b) emission cross sections of the $\text{Er}^{3+}: 4I_{13/2} \rightarrow 4I_{15/2}$ transition with the participation of m ($m = 0, 1$, and 2) phonons and absorption cross sections of the $\text{Ho}^{3+}: 5I_8 \rightarrow 5I_7$ transition in the silicate sample.

larger spectral overlap among them is determined after the matrix absorbs one or two phonons, as indicated in Fig. 9(a) and (b). In this case, the energy transfer microscopic parameter (C_{DA}) from Er^{3+} to Ho^{3+} can be estimated using Forster’s spectral overlap model given by^{32,40,41}.

$$C_{DA} = \frac{3c}{8\pi^4 n^2} \int \delta_{em}^D(\lambda) \delta_{abs}^A(\lambda) d\lambda \tag{9}$$

where c is the light speed in vacuum, n is the refractive index. σ_{abs} is the absorption cross section of $\text{Ho}^{3+}: 5I_8 \rightarrow 5I_6$ and $5I_8 \rightarrow 5I_7$ transitions, respectively.

Based on Eq. 9 and Fig. 9(a) and (b), the energy transfer microscopic parameter of ET2 process is as high as $5.52 \times 10^{-40} \text{ cm}^6 \cdot \text{s}^{-1}$, which is significantly larger than that of ET1 process ($0.66 \times 10^{-40} \text{ cm}^6 \cdot \text{s}^{-1}$) in the prepared sample. It is suggested that ET2 process is more efficient than ET1 process, which is in accordance with the results of Fig. 6(a) and (b). Furthermore, it further illustrates the enhanced $2\mu\text{m}$ emission can be mainly ascribed to ET2 process in the $\text{Er}^{3+}/\text{Ho}^{3+}$ codoped silicate glass. Finally, based on the analysis of the energy transfer mechanisms, the energy transfer microscopic parameters (C_{DA}) of ET2 process in silicate glass ($5.52 \times 10^{40} \text{ cm}^6/\text{s}$) is much higher than that of germanosilicate glass ($4.16 \times 10^{40} \text{ cm}^6/\text{s}$)³⁰, suggesting that more efficient energy transfer between them can be achieved in silicate glass. The result reveals that $\text{Er}^{3+}/\text{Ho}^{3+}$ codoped silicate glass possesses suitable phonon energy ($\sim 952 \text{ cm}^{-1}$) is a more promising material for improving the Ho^{3+} $2.0\mu\text{m}$ fiber laser performance.

Rate equation analysis. As previously stated, the fluorescent intensity become stronger with increasing Ho^{3+} concentration and then become weaker with a further enhancement of Ho^{3+} ions. Therefore, to better know the energy transfer process between Er^{3+} and Ho^{3+} and elucidate the $2\mu\text{m}$ fluorescence behaviors, the rate equation model between Er^{3+} and Ho^{3+} ions were developed according to energy level diagram of Fig. 5. Here, only ET2 process is considered because of much lower energy transfer probability of ET1, Furthermore, the excited state absorption (ESA), back transfer and energy transfer up-conversion (ETU) processes are neglected³⁰. In addition, the quenching effect of OH^- is neglected. Basing on $\text{Er}^{3+}: 4I_{15/2}, 4I_{13/2}, 4I_{11/2}$ levels and $\text{Ho}^{3+}: 5I_8$ levels, the rate equations can be built as follows:

$$\frac{dN_1}{dt} = -RN_1 + A_{31}N_3 + A_{21}N_2 + C_{ET}N_2N_{Ho} \tag{10}$$

$$\frac{dN_2}{dt} = A_{32}N_3 - A_{21}N_2 - C_{ET}N_2N_{Ho} \tag{11}$$

$$\frac{dN_3}{dt} = RN_1 - A_{31}N_3 - A_{32}N_3 \tag{12}$$

$$N_1 + N_2 + N_3 = N_{Er} \tag{13}$$

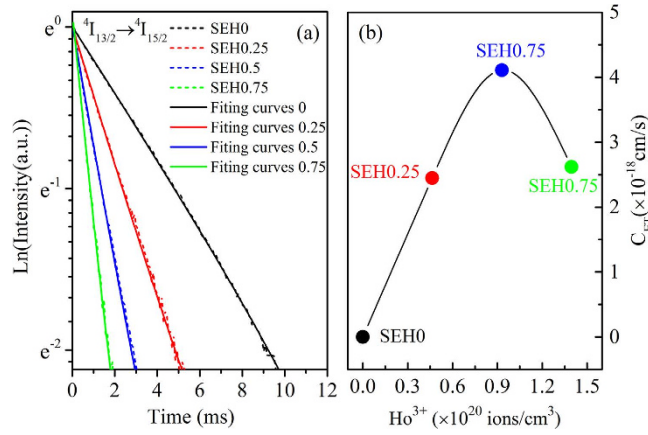


Figure 10. (a) Measured decay data of Er³⁺: ⁴I_{13/2} level and best fitting curves via rate equation in silicate glass; (b) calculated energy transfer rates derived from rate equation model and decay data.

where R is the pumping rate. A_{ij} is the spontaneous transition from levels i and j. C_{ET} is the energy transfer rate from Er³⁺: ⁴I_{13/2} to Ho³⁺: ⁵I₇ level. Moreover, the N₁, N₂, N₃, N_{Er} and N_{Ho} are the populations at the Er³⁺: ⁴I_{15/2}, ⁴I_{13/2}, ⁴I_{11/2}, total Er³⁺ and Ho³⁺: ⁵I₈ levels, respectively.

When pumping source is switched off, the following expression can be obtained by solving Es. (12) and as follow:

$$N_3(t) = N_3(0) \exp[-(A_{31} + A_{32})t] \quad (14)$$

The following equation can be obtained by combining with Eq. (11) and (14), N₂(t) can be expressed as

$$\frac{N_2(t)}{N_2(0)} = \left[1 - \frac{A_{32}N_3(0)}{N_2(0)[A_{21} + C_{ET}N_{Ho} - A_{31} - A_{32}]} \right] \exp[-(A_{21} + C_{ET}N_{Ho})t] + \frac{A_{32}N_3(0)}{N_2(0)[A_{21} + C_{ET}N_{Ho} - A_{31} - A_{32}]} \exp[-(A_{31} + A_{32})t] \quad (15)$$

where N₃(0) and N₂(0) is the excited population numbers in Er³⁺: ⁴I_{11/2} and ⁴I_{13/2} level, respectively, after the pump source turns off (t = 0).

By solving Eq. (11) in the steady state condition (dN₂(t)/dt = 0), the ratio of N₃(0) and N₂(0) can be derived as

$$\frac{N_3(0)}{N_2(0)} = \frac{A_{21} + C_{ET}N_{Ho}}{A_{32}} \quad (16)$$

Basing on Eq. (15) and (16), then the fitting functions of Er³⁺: ⁴I_{13/2} level can be determined as

$$\frac{N_2(t)}{N_2(0)} = \frac{A_{21} + C_{ET}N_{Ho}}{[A_{21} + C_{ET}N_{Ho} - A_{31} - A_{32}]} \exp[-(A_{31} + A_{32})t] - \frac{A_{31} + A_{32}}{[A_{21} + C_{ET}N_{Ho} - A_{31} - A_{32}]} \exp[-(A_{21} + C_{ET}N_{Ho})t] \quad (17)$$

Finally, The decay data of Er³⁺: ⁴I_{13/2} levels are best fitting curves via Eq. (17) as showed in Fig. 10(a). C_{ET} can be obtained by fitting the decay curve of the 1.53 μm emission (Er³⁺: ⁴I_{13/2} → ⁴I_{15/2}) and plotted in Fig. 10(b), which indicates that the energy transfer rate increases firstly and then decreases with increasing Ho³⁺ concentration. This tendency is in good agreement with the results of Fig. 2. Moreover, it is noticed the higher C_{ET} can be as high as 4.2 × 10⁻¹⁸ cm³/s. The higher C_{ET} is beneficial for population accumulation of Ho³⁺: ⁵I₇ level and improving corresponding 2 μm emissions. Therefore, it is expected that Ho³⁺ activated silicate glasses are promising candidates for 2 μm fiber laser.

Conclusions

In brief, Er³⁺/Ho³⁺ codoped silicate glasses with low OH⁻ absorption coefficient (0.23 cm⁻¹) were prepared. Absorption spectra were determined. Intense mid-infrared emissions near 2 μm are observed with optimal Ho₂O₃ concentration of 0.5 mol %. The spectral components of the 2 μm fluorescence band were analyzed and an equivalent model of four-level system was proposed to describe the 2 μm emission band. The prepared glass possesses high emission cross section (5.61 × 10⁻²¹ cm²), fluorescence lifetime (2.95 ms) for Ho³⁺: ⁵I₇ → ⁵I₈ transition. Moreover, the energy transfer mechanism was proposed according to the energy level diagram between the Er³⁺ and Ho³⁺ ions and 980 nm, 1.53 μm fluorescence were measured to illustrate energy transfer processes.

In addition, the energy transfer rate W_{ET} (1170.6 s^{-1}) and energy transfer efficiency η (85.9%) were quantitative analyzed from decay analysis of the Er^{3+} : ${}^4\text{I}_{13/2}$ level. Such high energy transfer efficiency was attributed to the excellent matching of the host phonon energy with the energy gap between the Er^{3+} : ${}^4\text{I}_{13/2}$ and Ho^{3+} : ${}^5\text{I}_7$ levels. Energy transfer microscopic parameters (C_{DA}) were calculated and quantitative analyzed by host-assisted spectral overlap function and further indicate the enhanced $2\text{ }\mu\text{m}$ emission can be mainly ascribed to ET2 process. Furthermore, rate equation model was developed to elucidate the observed $2\text{ }\mu\text{m}$ fluorescence behaviors with the change of Ho^{3+} concentration. Results demonstrate that $\text{Er}^{3+}/\text{Ho}^{3+}$ codoped silicate glass has potential application for $2\text{ }\mu\text{m}$ laser and may provide useful guidance for the design of other mid-infrared laser materials.

References

- Henderson, S. W. *et al.* Coherent laser radar at $2\text{ }\mu\text{m}$ using solid-state lasers. *IEEE Trans. Geosci. Rem. Sens.* **31**, 4–15 (1993).
- Agger, S., Povlsen, J. H. & Varming, P. Single-frequency thulium-doped distributed-feedback fiber laser. *Opt. Lett.* **29**, 1503–1505 (2004).
- Seddon, A. B., Tang, Z., Furniss, D., Sujecki, S. & Benson, T. M. Progress in rare-earth-doped mid-infrared fiber lasers. *Opt. Express*. **18**, 26704–26719 (2010).
- Kurkov, A., Dvoyrin, V. & Marakulin, A. All-fiber 10 W holmium lasers pumped at $\lambda = 1.15\text{ }\mu\text{m}$. *Opt. Lett.* **35**, 490–492 (2010).
- Yao, C. *et al.* Holmium-doped fluorotellurite microstructured fibers for $2.1\text{ }\mu\text{m}$ lasing. *Opt. Lett.* **40**, 4695–4698 (2015).
- Wen, X. *et al.* Highly Tm^{3+} doped germanate glass and its single mode fiber for $2.0\text{ }\mu\text{m}$ laser. *Sci. Rep.* **6** (2016).
- Hemming, A., Jackson, S. D., Sabella, A., Bennetts, S. & Lancaster, D. High power, narrow bandwidth and broadly tunable Tm^{3+} , Ho^{3+} co-doped aluminosilicate glass fibre laser. *Electron. Lett.* **46**, 1 (2010).
- Hemming, A., Simakov, N., Haub, J. & Carter, A. A review of recent progress in holmium-doped silica fibre sources. *Opt. Fiber Technol.* **20**, 621–630 (2014).
- Jackson, S. D. & King, T. A. High-power diode-cladding-pumped Tm-doped silica fiber laser. *Opt. Lett.* **23**, 1462–1464 (1998).
- Geng, J., Wang, Q., Luo, T., Jiang, S. & Amzajerdian, F. Single-frequency narrow-linewidth Tm-doped fiber laser using silicate glass fiber. *Opt. Lett.* **34**, 3493–3495 (2009).
- Wu, J., Yao, Z., Zong, J. & Jiang, S. Highly efficient high-power thulium-doped germanate glass fiber laser. *Opt. Lett.* **32**, 638–640 (2007).
- Yang, X., Huang, H., Shen, D., Zhu, H. & Tang, D. $2.1\text{ }\mu\text{m}$ Ho: LuAG ceramic laser intracavity pumped by a diode-pumped Tm: YAG laser. *Chin. Opt. Lett.* **12**, 121405–121405 (2014).
- Zhou, B., Pun, E. Y. B., Lin, H., Yang, D. L. & Huang, L. H. Judd-Ofelt analysis, frequency upconversion, and infrared photoluminescence of Ho^{3+} -doped and $\text{Ho}^{3+}/\text{Yb}^{3+}$ -codoped lead bismuth gallate oxide glasses. *J. Appl. Phys.* **106**, 103105 (2009).
- Wang, X., Lin, H., Yang, D. L., Lin, L. & Pun, E. Y. B. Optical transitions and upconversion fluorescence in $\text{Ho}^{3+}/\text{Yb}^{3+}$ doped bismuth tellurite glasses. *J. Appl. Phys.* **107**, 113535 (2007).
- Peng, Y.-P., Guo, Y., Zhang, J. & Zhang, L. $\text{Ho}^{3+}/\text{Yb}^{3+}$ -codoped germanate-tellurite glasses for $2.0\text{ }\mu\text{m}$ emission performance. *Appl. Opt.* **53**, 1564–1569 (2014).
- Liu, X., Huang, F., Cheng, J., Fan, X. & Chen, D. Investigation on $\text{Er}^{3+}/\text{Ho}^{3+}$ co-doped silicate glass for $\sim 2\text{ }\mu\text{m}$ fiber lasers. *J. Lumin.* **162**, 197–202 (2015).
- Li, M., Bai, G., Guo, Y., Hu, L. & Zhang, J. Investigation on Tm^{3+} -doped silicate glass for $1.8\text{ }\mu\text{m}$ emission. *J. Lumin.* **132**, 1830–1835 (2012).
- Wang, Q., Geng, J., Luo, T. & Jiang, S. Mode-locked $2\text{ }\mu\text{m}$ laser with highly thulium-doped silicate fiber. *Opt. Lett.* **34**, 3616–3618 (2009).
- Li, K., Zhang, G. & Hu, L. Watt-level $\sim 2\text{ }\mu\text{m}$ laser output in Tm^{3+} -doped tungsten tellurite glass double-cladding fiber. *Opt. Lett.* **35**, 4136–4138 (2010).
- Guo, C., Shen, D., Long, J. & Wang, F. High-power and widely tunable Tm-doped fiber laser at $2\text{ }\mu\text{m}$. *Chin. Opt. Lett.* **10**, 091406–091406 (2012).
- Lu, Y. *et al.* Ho^{3+} doped germanate-tellurite glass sensitized by Er^{3+} and Yb^{3+} for efficient $2.0\text{ }\mu\text{m}$ laser fiber. *Mater. Res. Bull.* **84**, 124–131 (2016).
- Balda, R., Lacha, L., Fernández, J., Arriandiaga, M. & Martin, D. Spectroscopic properties of the $1.4\text{ }\mu\text{m}$ emission of Tm^{3+} ions in $\text{TeO}_2\text{-WO}_3\text{-PbO}$ glasses. *Opt. Express*. **16**, 11836 (2008).
- Jlassi, I., Elhouichet, H., Ferid, M., Chtourou, R. & Oueslati, M. Study of photoluminescence quenching in Er^{3+} doped tellurite glasses. *Opt. Mater.* **32**, 743–747 (2010).
- Wen, X. *et al.* Tm^{3+} doped barium gallo-germanate glass single-mode fibers for $2.0\text{ }\mu\text{m}$ laser. *Opt. Express*. **23**, 7722–7731 (2015).
- Xu, R., Tian, Y., Hu, L. & Zhang, J. Efficient $\sim 2\text{ }\mu\text{m}$ emission and energy transfer mechanism of Ho^{3+} doped barium gallium germanate glass sensitized by Tm^{3+} ions. *Appl. Phys. B* **108**, 597–602 (2012).
- Payne, S. A., Chase, L., Smith, L. K., Kway, W. L. & Krupke, W. F. Infrared cross-section measurements for crystals doped with Er^{3+} , Tm^{3+} , and Ho^{3+} . *Quantum Electronics, IEEE*. **28**, 2619–2630 (1992).
- Li, M., Liu, X., Guo, Y., Hu, L. & Zhang, J. Energy transfer characteristics of silicate glass doped with Er^{3+} , Tm^{3+} , and Ho^{3+} for $\sim 2\text{ }\mu\text{m}$ emission. *J. Appl. Phys.* **114**, 243501 (2013).
- Xu, R., Wang, M., Tian, Y., Hu, L. & Zhang, J. $2.05\text{ }\mu\text{m}$ emission properties and energy transfer mechanism of germanate glass doped with Ho^{3+} , Tm^{3+} , and Er^{3+} . *J. Appl. Phys.* **109**, 053503 (2011).
- Xu, R., Tian, Y., Wang, M., Hu, L. & Zhang, J. Investigation on broadband near-infrared emission and energy transfer in $\text{Er}^{3+}\text{-Tm}^{3+}$ codoped germanate glasses. *Opt. Mater.* **33**, 299–302 (2011).
- Wei, T. *et al.* Quantitative Analysis of Energy Transfer and Origin of Quenching in $\text{Er}^{3+}/\text{Ho}^{3+}$ Codoped Germanosilicate Glasses. *J. Phys. Chem. A*. **119**, 6823–6830 (2015).
- Tao, L., Tsang, Y. H., Zhou, B., Richards, B. & Jha, A. Enhanced $2.0\text{ }\mu\text{m}$ emission and energy transfer in $\text{Yb}^{3+}/\text{Ho}^{3+}/\text{Ce}^{3+}$ triply doped tellurite glass. *J. Non-Cryst. Solids*. **358**, 1644–1648 (2012).
- Gao, G. & Wondraczek, L. Near-infrared down-conversion in $\text{Mn}^{2+}\text{-Yb}^{3+}$ co-doped Zn_2GeO_4 . *J. Mater. Chem. C*. **1**, 1952–1958 (2013).
- Gao, G. & Wondraczek, L. Near-infrared downconversion in $\text{Pr}^{3+}/\text{Yb}^{3+}$ co-doped boro-aluminosilicate glasses and LaBO_3 glass ceramics. *Opt. Mater. Expre.* **3**, 633–644 (2013).
- Gao, G., Peng, M. & Wondraczek, L. Spectral shifting and NIR down-conversion in $\text{Bi}^{3+}/\text{Yb}^{3+}$ co-doped Zn_2GeO_4 . *J. Mater. Chem. C*. **2**, 8083–8088 (2014).
- Ma, Y., Huang, F., Hu, L. & Zhang, J. $\text{Er}^{3+}/\text{Ho}^{3+}$ -Codoped Fluorotellurite Glasses for $2.7\text{ }\mu\text{m}$ Fiber Laser. *Mater. Fibers*. **1**, 11–20 (2013).
- Huang, F., Liu, X., Li, W., Hu, L. & Chen, D. Energy transfer mechanism in Er^{3+} doped fluoride glass sensitized by Tm^{3+} or Ho^{3+} for $2.7\text{ }\mu\text{m}$ emission. *Chin. Opt. Lett.* **12**, 051601 (2014).
- Tian, Y., Jing, X. & Xu, S. Spectroscopic analysis and efficient diode-pumped $2.0\text{ }\mu\text{m}$ emission in $\text{Ho}^{3+}/\text{Tm}^{3+}$ codoped fluoride glass. *Spectrochim. Acta, Part A*. **115**, 33–38 (2013).

38. Balaji, S., Sontakke, A. D., Sen, R. & Kalyandurg, A. Efficient ~ 2.0 μm emission from Ho^{3+} doped tellurite glass sensitized by Yb^{3+} ions: Judd-Ofelt analysis and energy transfer mechanism. *Opt. Mater. Express*. **1**, 138–150 (2011).
39. Zhang, W. J., Chen, Q. J., Qian, Q. & Zhang, Q. Y. The 1.2 and 2.0 μm Emission from Ho^{3+} in Glass Ceramics Containing BaF_2 Nanocrystals. *J. Am. Ceram. Soc.* **95**, 663–669 (2012).
40. Sontakke, A. D., Biswas, K., Mandal, A. K. & Annapurna, K. Concentration quenched luminescence and energy transfer analysis of Nd^{3+} ion doped Ba-Al-metaphosphate laser glasses. *Appl. Phys. B*. **101**, 235–244 (2010).
41. Balaji, S. & Mandal, A. K. & Annapurna, K. Energy transfer based NIR to visible upconversion: Enhanced red luminescence from $\text{Yb}^{3+}/\text{Ho}^{3+}$ co-doped tellurite glass. *Opt. Mater.* **34**, 1930–1934 (2012).

Acknowledgements

This research was financially supported by the Chinese National Natural Science Foundation (No. 51372235, 51272243, 51472225 and 61308090), Zhejiang Provincial Natural Science Foundation of China (No. LR14E020003), the International Science & Technology Cooperation Program of China (Grant no. 2013DFE63070), and Public Technical International Cooperation project of Science Technology Department of Zhejiang Province (2015c340009).

Author Contributions

R.J.C. wrote the main manuscript text. Y.T., F.F.H. and Y.Y.G. checked up. Y.L. is responsible for the experiment. S.Q.X. and J.J. Zhang proposed valuable suggestions for our manuscript. All authors reviewed the manuscript.

Additional Information

Competing financial interests: The authors declare no competing financial interests.

How to cite this article: Cao, R. *et al.* 2 μm emission properties and nonresonant energy transfer of Er^{3+} and Ho^{3+} codoped silicate glasses. *Sci. Rep.* **6**, 37873; doi: 10.1038/srep37873 (2016).

Publisher's note: Springer Nature remains neutral with regard to jurisdictional claims in published maps and institutional affiliations.



This work is licensed under a Creative Commons Attribution 4.0 International License. The images or other third party material in this article are included in the article's Creative Commons license, unless indicated otherwise in the credit line; if the material is not included under the Creative Commons license, users will need to obtain permission from the license holder to reproduce the material. To view a copy of this license, visit <http://creativecommons.org/licenses/by/4.0/>

© The Author(s) 2016